Supplement of Absolute and Relative Pose Estimation in Refractive Multi View

Xiao Hu[1,2], François Lauze[2], Kim Steenstrup Pedersen[2,3], and Jean Mélou[4]
[1]: DTU Space, Technical University of Denmark, Lyngby, Denmark
[2]: Department of Computer Science (DIKU), University of Copenhagen, Denmark
[3]: Natural History Museum of Denmark (NHMD), University of Copenhagen, Denmark
[4]: IRIT, UMR CNRS 5505, Toulouse, France
xiahaa@space.dtu.dk, francois@diku.dk, kimstp@di.ku.dk, jean.melou@toulouse-inp.fr

1. Jacobian Matrices related to Pose Estimation under Refraction

This appendix section gives the Jacobian matrices derived for pose estimation under refraction.

1.1. Absolute Pose Refinement

By using the chain rule, we have the Jacobian matrix w.r.t $\mathbf{R}$ and $\mathbf{c}$ as

$$\begin{aligned}\mathbf{J}_{\mathbf{R}} &= \mathbf{J}_{\mathbf{l}_\mathrm{I}(1,2,3)}\mathbf{J}_{\mathbf{R}}^{\mathbf{l}_\mathrm{I}(1,2,3)} + \mathbf{J}_{\mathbf{l}_\mathrm{I}(4,5,6)}\mathbf{J}_{\mathbf{R}}^{\mathbf{l}_\mathrm{I}(4,5,6)}\,,\\ \mathbf{J}_{\mathbf{c}} &= \mathbf{J}_{\mathbf{l}_\mathrm{I}(1,2,3)}\mathbf{J}_{\mathbf{c}}^{\mathbf{l}_\mathrm{I}(1,2,3)} + \mathbf{J}_{\mathbf{l}_\mathrm{I}(4,5,6)}\mathbf{J}_{\mathbf{c}}^{\mathbf{l}_\mathrm{I}(4,5,6)}\,.\end{aligned} \tag{1}$$

where $\mathbf{J}_{\mathbf{l}_\mathrm{I}(1,2,3)} = -\mathbf{p}_\mathrm{I}^\wedge$ and $\mathbf{J}_{\mathbf{l}_\mathrm{I}(4,5,6)} = \mathbf{I}$. Here $\mathbf{a}^\wedge$ represents the skew-symmetric matrix of a vector $\mathbf{a}$. Since $\mathbf{R}$ and $\mathbf{c}$ are embedded in $\mathbf{l}_\mathrm{I}$, again, by the chain rule, we have:

$$\begin{aligned}\mathbf{J}_{\mathbf{R}}^{\mathbf{l}(1,2,3)} &= \mathbf{J}_{\mathbf{q}_\mathrm{I}}^{\mathbf{l}(1,2,3)}\mathbf{J}_{\mathbf{q}_\mathrm{I}}^{\mathbf{q}_\mathrm{I}}\mathbf{J}_{\mathbf{R}}^{\mathbf{q}_\mathrm{I}} + \mathbf{J}_{\mathbf{r}_\mathrm{I}}^{\mathbf{l}(1,2,3)}\mathbf{J}_{\mathbf{q}_\mathrm{I}}^{\mathbf{r}_\mathrm{I}}\mathbf{J}_{\mathbf{R}}^{\mathbf{q}_\mathrm{I}},\\ \mathbf{J}_{\mathbf{c}}^{\mathbf{l}(1,2,3)} &= \mathbf{J}_{\mathbf{q}_\mathrm{I}}^{\mathbf{l}(1,2,3)}\mathbf{J}_{{}^\mathrm{I}\mathbf{c}_\mathrm{C}}^{\mathbf{q}_\mathrm{I}}\mathbf{J}_{\mathbf{c}}^{{}^\mathrm{I}\mathbf{c}_\mathrm{C}},\\ \mathbf{J}_{\mathbf{R}}^{\mathbf{l}(4,5,6)} &= \mathbf{J}_{\mathbf{q}_\mathrm{I}}^{\mathbf{l}(4,5,6)}\mathbf{J}_{\mathbf{q}_\mathrm{I}}^{\mathbf{q}_\mathrm{I}}\mathbf{J}_{\mathbf{R}}^{\mathbf{q}_\mathrm{I}} + \mathbf{J}_{\mathbf{r}_\mathrm{I}}^{\mathbf{l}(4,5,6)}\mathbf{J}_{\mathbf{q}_\mathrm{I}}^{\mathbf{r}_\mathrm{I}}\mathbf{J}_{\mathbf{R}}^{\mathbf{q}_\mathrm{I}},\\ \mathbf{J}_{\mathbf{c}}^{\mathbf{l}(4,5,6)} &= \mathbf{J}_{\mathbf{q}_\mathrm{I}}^{\mathbf{l}(4,5,6)}\mathbf{J}_{{}^\mathrm{I}\mathbf{c}_\mathrm{C}}^{\mathbf{q}_\mathrm{I}}\mathbf{J}_{\mathbf{c}}^{{}^\mathrm{I}\mathbf{c}_\mathrm{C}},\end{aligned} \tag{2}$$

where

$$\begin{aligned}\mathbf{J}_{\mathbf{q}_\mathrm{I}}^{\mathbf{l}_\mathrm{I}(1,2,3)} &= [\mathbf{0} \quad \mathbf{r}_\mathrm{I}]\,, \quad \mathbf{J}_{\mathbf{r}_\mathrm{I}}^{\mathbf{l}_\mathrm{I}(1,2,3)} = [\mathbf{q}_\mathrm{I}(4)\mathbf{I} \quad \mathbf{0}]\,,\\ \mathbf{J}_{\mathbf{q}_\mathrm{I}}^{\mathbf{l}_\mathrm{I}(4,5,6)} &= [-\mathbf{r}_\mathrm{I}^\wedge \quad \mathbf{0}], \quad \mathbf{J}_{\mathbf{r}_\mathrm{I}}^{\mathbf{l}_\mathrm{I}(4,5,6)} = [\mathbf{q}_\mathrm{I}^\wedge \quad \mathbf{0}\,]\,,\\ \mathbf{J}_{\mathbf{q}_\mathrm{I}}^{\mathbf{q}_\mathrm{I}} &= \begin{bmatrix} -{}^\mathrm{I}\mathbf{c}_\mathrm{C}(3) & 0 & {}^\mathrm{I}\mathbf{c}_\mathrm{C}(1)\\ 0 & -{}^\mathrm{I}\mathbf{c}_\mathrm{C}(3) & {}^\mathrm{I}\mathbf{c}_\mathrm{C}(2)\\ 0 & 0 & 0\\ 0 & 0 & 1\end{bmatrix},\end{aligned} \tag{3}$$

$$\begin{aligned}\mathbf{J}_{{}^\mathrm{I}\mathbf{c}_\mathrm{C}}^{\mathbf{q}_\mathrm{I}} &= \begin{bmatrix} \mathbf{q}_\mathrm{I}(3) & 0 & -\mathbf{q}_\mathrm{I}(1)\\ 0 & \mathbf{q}_\mathrm{I}(3) & -\mathbf{q}_\mathrm{I}(2)\\ 0 & 0 & 0\\ 0 & 0 & 0\end{bmatrix},\\ \mathbf{J}_{\mathbf{q}_\mathrm{I}}^{\mathbf{r}_\mathrm{I}} &= \begin{bmatrix} \lambda & 0 & 0\\ 0 & \lambda & 0\\ 0 & 0 & \frac{\lambda^2\mathbf{q}_\mathrm{I}(3)}{\mathbf{r}_\mathrm{I}(3)}\\ 0 & 0 & 0\end{bmatrix},\\ \mathbf{J}_{\mathbf{R}}^{\mathbf{q}_\mathrm{I}} &= \left({}^\mathrm{W}\mathbf{R}_\mathrm{I}^\top\mathbf{q}_\mathrm{W}\right)^\wedge, \quad \mathbf{J}_{\mathbf{c}}^{{}^\mathrm{I}\mathbf{c}_\mathrm{C}} = {}^\mathrm{W}\mathbf{R}_\mathrm{I}^\top\,.\end{aligned} \tag{4}$$

1.2. Relative Pose Refinement

Recall the refractive epipolar constraint given as

$$\mathbf{f}_{\mathrm{EC}} = {\mathbf{r}_\mathrm{I}^2}^\top({}^\mathrm{I}\mathbf{c}_\mathrm{V}^2 - {}^\mathrm{I}\,\mathbf{c}_\mathrm{V}^1)^\wedge\mathbf{r}_\mathrm{I}^1\,, \tag{5}$$

using the chain rule, we have the Jacobian matrices w.r.t $\mathbf{R}$, $\mathbf{c}$, and $\mathbf{p}$ as

$$\begin{aligned}\mathbf{J}_{\mathrm{EC}_\mathbf{x}} &= [\mathbf{J}_{\mathbf{R}}, \mathbf{J}_{\mathbf{c}}, \mathbf{0}]\,,\\ \mathbf{J}_{\mathbf{R}} &= \mathbf{J}_{\mathbf{r}_\mathrm{I}^2}\mathbf{J}_{\mathbf{R}}^{\mathbf{r}_\mathrm{I}^2} + \mathbf{J}_{{}^\mathrm{I}\mathbf{c}_\mathrm{V}^2}\mathbf{J}_{\mathbf{R}}^{{}^\mathrm{I}\mathbf{c}_\mathrm{V}^2}\,,\\ \mathbf{J}_{\mathbf{c}} &= \mathbf{J}_{{}^\mathrm{I}\mathbf{c}_\mathrm{V}^2}\mathbf{J}_{\mathbf{c}}^{{}^\mathrm{I}\mathbf{c}_\mathrm{V}^2}\,.\end{aligned} \tag{6}$$

where

$$\begin{aligned}\mathbf{J}_{\mathbf{r}_\mathrm{I}^2} &= \left(({}^\mathrm{I}\mathbf{c}_\mathrm{V}^2 - {}^\mathrm{I}\,\mathbf{c}_\mathrm{V}^1)^\wedge\mathbf{r}_\mathrm{I}^1\right)^\top,\\ \mathbf{J}_{{}^\mathrm{I}\mathbf{c}_\mathrm{V}^2} &= -{\mathbf{r}_\mathrm{I}^2}^\top(\mathbf{r}_\mathrm{I}^1)^\wedge\,,\\ \mathbf{J}_{\mathbf{R}}^{\mathbf{r}_\mathrm{I}^2} &= \mathbf{J}_{\mathbf{q}_\mathrm{I}}^{\mathbf{r}_\mathrm{I}^2}\mathbf{J}_{\mathbf{R}}^{\mathbf{q}_\mathrm{I}}\,,\\ \mathbf{J}_{\mathbf{R}}^{{}^\mathrm{I}\mathbf{c}_\mathrm{V}^2} &= \mathbf{J}_{\mathbf{q}_\mathrm{I}}^{{}^\mathrm{I}\mathbf{c}_\mathrm{V}^2}\mathbf{J}_{\mathbf{R}}^{\mathbf{q}_\mathrm{I}}\,,\\ \mathbf{J}_{\mathbf{c}}^{{}^\mathrm{I}\mathbf{c}_\mathrm{V}^2} &= \mathbf{J}_{{}^\mathrm{I}\mathbf{c}_\mathrm{C}}^{{}^\mathrm{I}\mathbf{c}_\mathrm{V}^2}\mathbf{J}_{\mathbf{c}}^{{}^\mathrm{I}\mathbf{c}_\mathrm{C}}\,.\end{aligned} \tag{7}$$

Similarly, for the reprojection error given as

$$\mathbf{f}_{\mathrm{RE}} = \begin{bmatrix} f_\mathrm{V}\frac{\mathbf{p}_\mathrm{V}(1)}{\mathbf{p}_\mathrm{V}(3)} - f_\mathrm{V}\frac{\mathbf{r}_\mathrm{V}(1)}{\mathbf{r}_\mathrm{V}(3)}\\ f_\mathrm{V}\frac{\mathbf{p}_\mathrm{V}(2)}{\mathbf{p}_\mathrm{V}(3)} - f_\mathrm{V}\frac{\mathbf{r}_\mathrm{V}(2)}{\mathbf{r}_\mathrm{V}(3)}\end{bmatrix}, \tag{8}$$

using the chain rule, we have the Jacobian matrices w.r.t $\mathbf{R}$, $\mathbf{c}$, and $\mathbf{p}$ as

$$\begin{aligned}\mathbf{J}_{\mathrm{RE}_\mathbf{x}} &= [\mathbf{J}_\mathbf{R}, \mathbf{J}_\mathbf{c}, \mathbf{J}_\mathbf{p}] \,, \\ \mathbf{J}_\mathbf{R} &= \mathbf{J}_{\mathbf{p}_\mathrm{V}} \mathbf{J}_\mathbf{R}^{\mathbf{p}_\mathrm{V}} + \mathbf{J}_{\mathbf{r}_\mathrm{V}} \mathbf{J}_\mathbf{R}^{\mathbf{r}_\mathrm{V}} \,, \\ \mathbf{J}_\mathbf{c} &= \mathbf{J}_{\mathbf{p}_\mathrm{V}} \mathbf{J}_\mathbf{c}^{\mathbf{p}_\mathrm{V}} + \mathbf{J}_{\mathbf{r}_\mathrm{V}} \mathbf{J}_\mathbf{c}^{\mathbf{r}_\mathrm{V}} \,, \\ \mathbf{J}_\mathbf{p} &= \mathbf{J}_{\mathbf{p}_\mathrm{V}} \mathbf{J}_\mathbf{p}^{\mathbf{p}_\mathrm{V}} \,,\end{aligned} \tag{9}$$

where

$$\begin{aligned}\mathbf{J}_{\mathbf{p}_\mathrm{V}} &= \begin{bmatrix} f_\mathrm{V} \frac{1}{\mathbf{p}_\mathrm{V}(3)} & 0 & -f_\mathrm{V} \frac{\mathbf{p}_\mathrm{V}(1)}{\mathbf{p}_\mathrm{V}(3)^2} \\ 0 & f_\mathrm{V} \frac{1}{\mathbf{p}_\mathrm{V}(3)} & -f_\mathrm{V} \frac{\mathbf{p}_\mathrm{V}(2)}{\mathbf{p}_\mathrm{V}(3)^2} \end{bmatrix} \,, \\ \mathbf{J}_{\mathbf{r}_\mathrm{V}} &= \begin{bmatrix} -f_\mathrm{V} \frac{1}{\mathbf{r}_\mathrm{V}(3)} & 0 & f_\mathrm{V} \frac{\mathbf{r}_\mathrm{V}(1)}{\mathbf{r}_\mathrm{V}(3)^2} \\ 0 & -f_\mathrm{V} \frac{1}{\mathbf{r}_\mathrm{V}(3)} & f_\mathrm{V} \frac{\mathbf{r}_\mathrm{V}(2)}{\mathbf{r}_\mathrm{V}(3)^2} \end{bmatrix} \,, \\ \mathbf{J}_\mathbf{R}^{\mathbf{p}_\mathrm{V}} &= \mathbf{J}_{{}^\mathrm{I}\mathbf{c}_\mathrm{V}}^{\mathbf{p}_\mathrm{V}} \mathbf{J}_\mathbf{R}^{{}^\mathrm{I}\mathbf{c}_\mathrm{V}^2} \,, \quad \mathbf{J}_\mathbf{R}^{\mathbf{r}_\mathrm{V}} = \mathbf{J}_{\mathbf{q}_\mathrm{I}}^{\mathbf{r}_\mathrm{V}} \mathbf{J}_\mathbf{R}^{\mathbf{q}_\mathrm{I}} \,, \quad \mathbf{J}_\mathbf{p}^{\mathbf{p}_\mathrm{V}} = \mathbf{I} \,, \\ \mathbf{J}_\mathbf{c}^{\mathbf{p}_\mathrm{V}} &= \mathbf{J}_{{}^\mathrm{I}\mathbf{c}_\mathrm{V}}^{\mathbf{p}_\mathrm{V}} \mathbf{J}_{{}^\mathrm{I}\mathbf{c}_\mathrm{C}}^{{}^\mathrm{I}\mathbf{c}^i\mathrm{V}} \mathbf{J}_\mathbf{c}^{{}^\mathrm{I}\mathbf{c}_\mathrm{C}} \,, \quad \mathbf{J}_\mathbf{c}^{\mathbf{r}_\mathrm{V}} = \mathbf{J}_{\mathbf{q}_\mathrm{I}}^{\mathbf{r}_\mathrm{V}} \mathbf{J}_{{}^\mathrm{I}\mathbf{c}_\mathrm{C}}^{\mathbf{q}_\mathrm{I}} \mathbf{J}_\mathbf{c}^{{}^\mathrm{I}\mathbf{c}_\mathrm{C}} \,.\end{aligned} \tag{10}$$

Some intermediate Jacobian matrices in (7) and (10) are given as follows:

$$\begin{aligned}\mathbf{J}_\mathbf{R}^{\mathbf{r}_\mathrm{I}^2} &= \mathbf{J}_{\mathbf{q}_\mathrm{I}}^{\mathbf{r}_\mathrm{I}^2} \mathbf{J}_\mathbf{R}^{\mathbf{q}_\mathrm{I}} \,, \\ \mathbf{J}_\mathbf{R}^{{}^\mathrm{I}\mathbf{c}_\mathrm{V}^2} &= \mathbf{J}_{\mathbf{q}_\mathrm{I}}^{{}^\mathrm{I}\mathbf{c}_\mathrm{V}^2} \mathbf{J}_\mathbf{R}^{\mathbf{q}_\mathrm{I}} \,, \\ \mathbf{J}_\mathbf{c}^{{}^\mathrm{I}\mathbf{c}_\mathrm{V}^2} &= \mathbf{J}_{{}^\mathrm{I}\mathbf{c}_\mathrm{C}}^{{}^\mathrm{I}\mathbf{c}_\mathrm{V}^2} \mathbf{J}_\mathbf{c}^{{}^\mathrm{I}\mathbf{c}_\mathrm{C}} \,,\end{aligned} \tag{11}$$

where

$$\begin{aligned}\mathbf{J}_{{}^\mathrm{I}\mathbf{c}_\mathrm{C}}^{\mathbf{q}_\mathrm{I}} &= \begin{bmatrix} 1 & 0 & -\frac{\mathbf{q}_\mathrm{I}(1)}{\mathbf{q}_\mathrm{I}(3)} \\ 0 & 1 & -\frac{\mathbf{q}_\mathrm{I}(2)}{\mathbf{q}_\mathrm{I}(3)} \\ 0 & 0 & 0 \end{bmatrix} \,, \\ \mathbf{J}_{\mathbf{q}_\mathrm{I}}^{\mathbf{q}_\mathrm{I}} &= \begin{bmatrix} -\frac{{}^\mathrm{I}\mathbf{c}_\mathrm{C}(3)}{\mathbf{q}_\mathrm{I}(3)} & 0 & {}^\mathrm{I}\mathbf{c}_\mathrm{C}(3) \frac{\mathbf{q}_\mathrm{I}(1)}{\mathbf{q}_\mathrm{I}(3)^2} \\ 0 & -\frac{{}^\mathrm{I}\mathbf{c}_\mathrm{C}(3)}{\mathbf{q}_\mathrm{I}(3)} & {}^\mathrm{I}\mathbf{c}_\mathrm{C}(3) \frac{\mathbf{q}_\mathrm{I}(2)}{\mathbf{q}_\mathrm{I}(3)^2} \\ 0 & 0 & 0 \end{bmatrix} \,, \\ \mathbf{J}_{\mathbf{q}_\mathrm{I}}^{\mathbf{r}^i\mathrm{I}} &= \begin{bmatrix} \lambda & 0 & 0 \\ 0 & \lambda & 0 \\ 0 & 0 & \frac{\lambda^2 \mathbf{q}_\mathrm{I}(3)}{\gamma} \end{bmatrix} \,, \\ \mathbf{J}_{\mathbf{q}_\mathrm{I}}^{{}^\mathrm{I}\mathbf{c}^i\mathrm{V}} &= \begin{bmatrix} 0 & 0 & 0 \\ 0 & 0 & 0 \\ 0 & 0 & \frac{-{}^\mathrm{I}\mathbf{c}_\mathrm{C}(3))(1-\lambda^2)}{\lambda \mathbf{q}_\mathrm{I}(3)^2 \gamma} \end{bmatrix} \,, \\ \mathbf{J}_{{}^\mathrm{I}\mathbf{c}_\mathrm{C}}^{{}^\mathrm{I}\mathbf{c}^i\mathrm{V}} &= \begin{bmatrix} 1 & 0 & 0 \\ 0 & 1 & 0 \\ 0 & 0 & \frac{1}{\lambda \mathbf{q}_\mathrm{I}(3)} \gamma \end{bmatrix} \,, \\ \mathbf{J}_\mathbf{R}^{\mathbf{q}_\mathrm{I}} &= \left({}^\mathrm{W}\mathbf{R}_\mathrm{I}^\top \mathbf{q}_\mathrm{W}\right)^\wedge \,, \quad \mathbf{J}_\mathbf{c}^{{}^\mathrm{I}\mathbf{c}_\mathrm{C}} = {}^\mathrm{W}\mathbf{R}_\mathrm{I}^\top \,, \\ \mathbf{J}_{{}^\mathrm{I}\mathbf{c}_\mathrm{V}}^{\mathbf{p}_\mathrm{V}} &= -\mathbf{I} \,, \quad \mathbf{J}_{\mathbf{q}_\mathrm{I}}^{\mathbf{r}_\mathrm{V}} = \mathbf{I} \,.\end{aligned} \tag{12}$$

where $\gamma = \sqrt{(1-\lambda^2) + \lambda^2 \mathbf{q}_\mathrm{I}(3)^2}$.

2. Setup of Synthetic Simulation

Fig. 1 show how the data are generated to evaluate the absolute pose solvers in the non planar and planar cases.

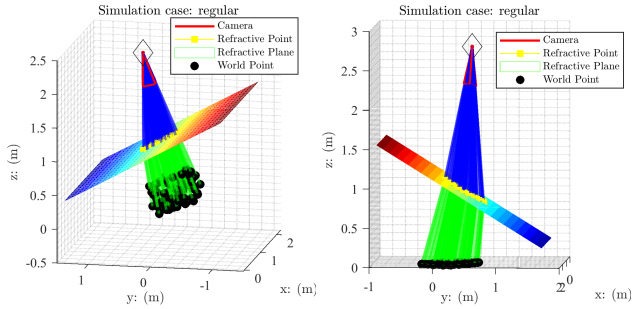

Figure 1. Simulation setup for absolute pose estimation: The left figure shows the setup for generating data (world points, image points, camera pose) under refraction for the non planar case. The right figure shows the setup for generating data for the planar case.

Fig. 2 show how the data are generated to evaluate the relative pose solvers.

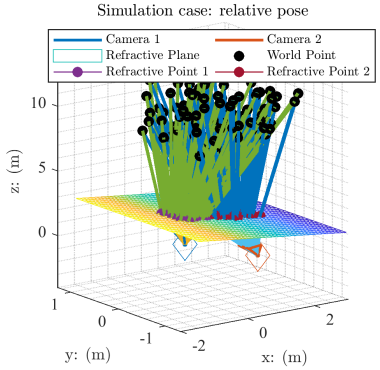

Figure 2. Simulation setup for relative pose estimation: The figure shows the setup for generating data (world points, image points, camera pose) under refraction.

Figure 3. Illustration of estimating refractive surface normal.

2.1. Zoom-out Results

Fig. 4, Fig. 5, and Fig. 6 demonstrate the synthetic experimental results, which are the zoom-out images corresponding to Fig. 7, 8, and 9 listed in the paper.

3. Supplementary Details for Real Data Experiment

This section presents supplementary details for the experiment described in Section 5.3 and Section 5.4 in the main paper.

3.1. Bathtub Dataset

The refractive index of water is set to 1.333. The submerged checker pattern was segmented out of raw images, as demonstrated in Fig. 7. We employed the estimated camera poses for a semi-dense 3D reconstruction of the submerged checker pattern, where the optical flow algorithm proposed by [2] was used to establish feature correspondences.

In Fig. 8, we show a refractive SfM reconstruction of the submerged checker pattern. We tried to apply a classical SfM reconstruction using the COLMAP software [3]. Unfortunately, it failed to give a sparse reconstruction result, whereas our method was able to reproduce the 3D structure of the submerged checker pattern.

3.2. Stag Beetle Dataset

The refractive index of the crystal resin is set to 1.6. We segmented the refractive parts from raw images on which the proposed algorithms were then executed, as demonstrated in Fig. 9. The surface normal was estimated using ArUco [1] fiducial markers glued on the surface, as shown in Fig. 3. Note that, in scenario 2, we only need to estimate it once.

Fig. 10 shows two representative side-view images of the real stag beetle dataset. They are given here to help readers visually evaluate the quality of the 3D reconstruction. As shown in Figure 11 in the main paper and in Fig. 11, the classical reconstruction fails to get the depth correct and produces an almost flat reconstruction, whereas our method more faithfully reproduce the 3D structure of the stag beetle (especially the legs and their attachment on the body).

3.3. Whiskey Bottle Dataset

We carried out an additional real experiment where we used a mobile phone camera to photograph a cylindrical whiskey bottle container placed at the bottom of a bathtub filled with water, as shown in Fig. 12. Similarly, we segmented the refractive parts from raw images on which the proposed algorithms were then executed. In Fig. 13, we show a refractive SfM reconstruction of the submerged whiskey bottle and the tray.

References

[1] Sergio Garrido-Jurado, Rafael Munoz-Salinas, Francisco José Madrid-Cuevas, and Rafael Medina-Carnicer. Generation of fiducial marker dictionaries using mixed integer linear programming. *Pattern Recognition*, 51:481–491, 2016. 3

[2] Till Kroeger, Radu Timofte, Dengxin Dai, and Luc Van Gool. Fast optical flow using dense inverse search. In *Proceedings of the European Conference on Computer Vision*, pages 471–488. Springer, 2016. 3

[3] Johannes L Schonberger and Jan-Michael Frahm. Structure-from-motion revisited. In *Proceedings of the IEEE Conference on Computer Vision and Pattern Recognition*, pages 4104–4113, 2016. 3, 7

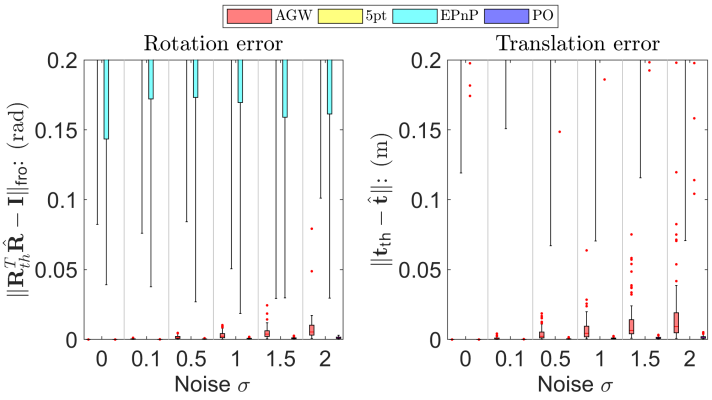

Figure 4. Comparison of absolute pose solvers for scenario 2 with respect to varying noise levels in the nonplanar case: the left box plot shows rotation error; the right box plot shows the translation error.

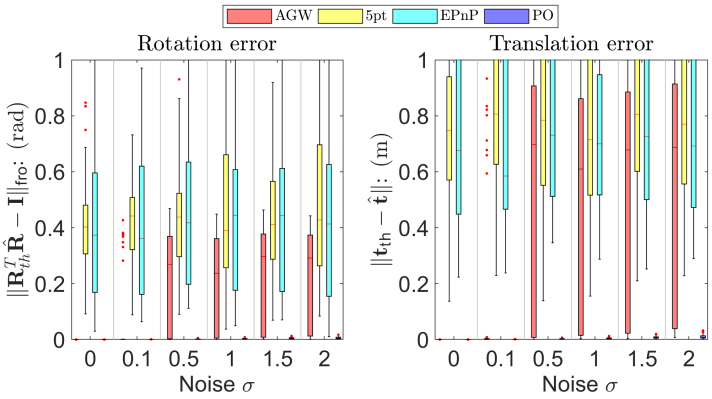

Figure 5. Comparison of absolute pose solvers for scenario 2 with respect to varying noise levels in the planar case: the left box plot shows rotation error; the right box plot shows the translation error.

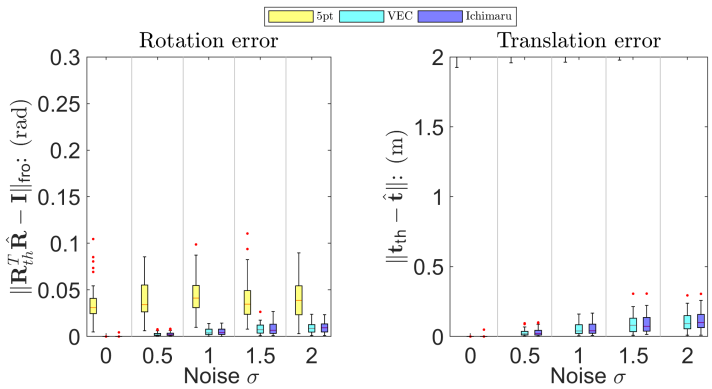

Figure 6. Comparison of relative pose solvers for scenario 2 with respect to varying noise levels: the left box plot shows rotation error; the right box plot shows the translation error.

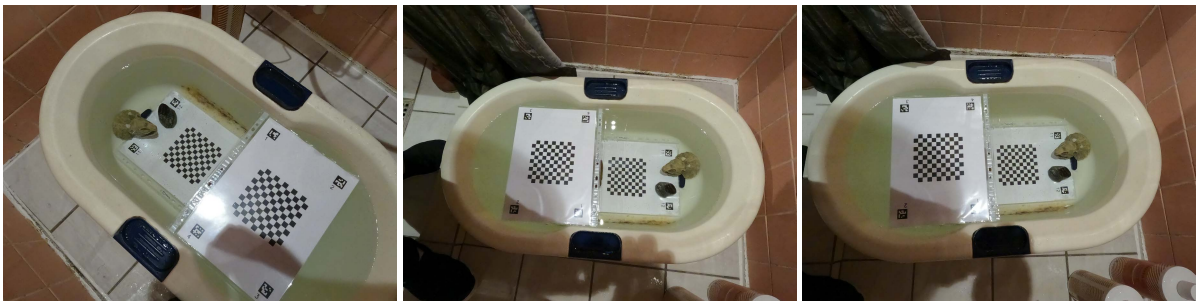

(a): Raw images.

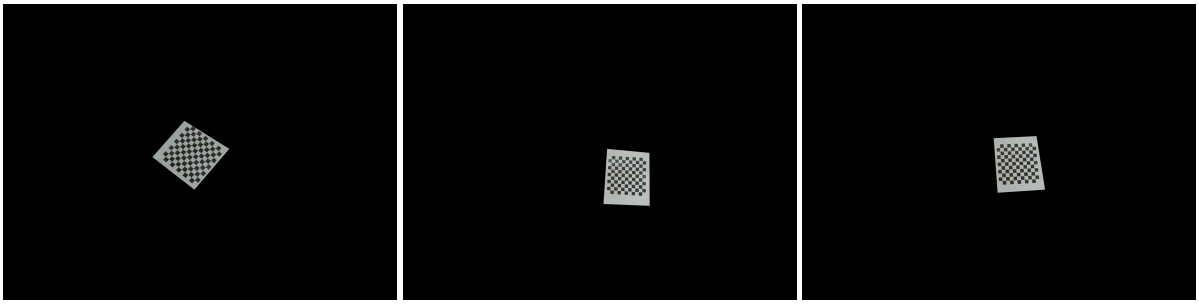

(b): Segmented refractive images.

Figure 7. Representative raw and segmented refractive images of the bathtub dataset used for 3D reconstruction.

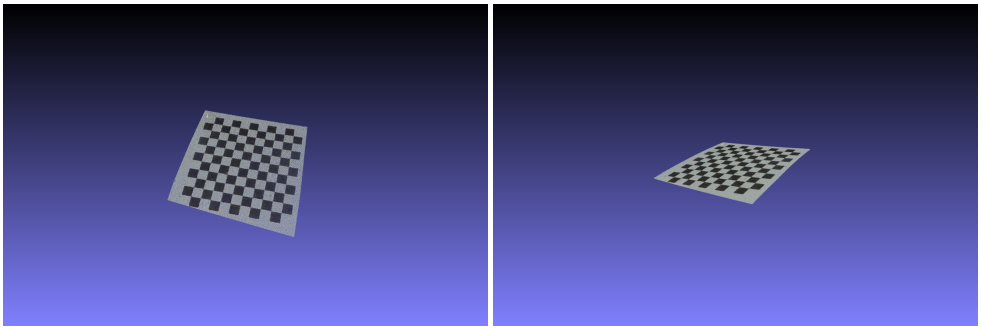

Figure 8. Representative side-view images of the real stag beetle dataset.

(a): Raw images.

(b): Segmented refractive images.

Figure 9. Representative raw and segmented refractive images of the real stag beetle dataset used for 3D reconstruction.

Figure 10. Representative side-view images of the real stag beetle dataset.

Figure 11. Supplementary SfM reconstructions based on 30 images, see Fig. 1. (Left) SfM reconstruction based on refractive SfM using our method for Scenario 2. (Right) SfM reconstruction based on perspective camera using COLMAP [3].

(a): Raw images.

(b): Segmented refractive images.

Figure 12. Representative raw and segmented refractive images of the real whisky bottle dataset used for 3D reconstruction.

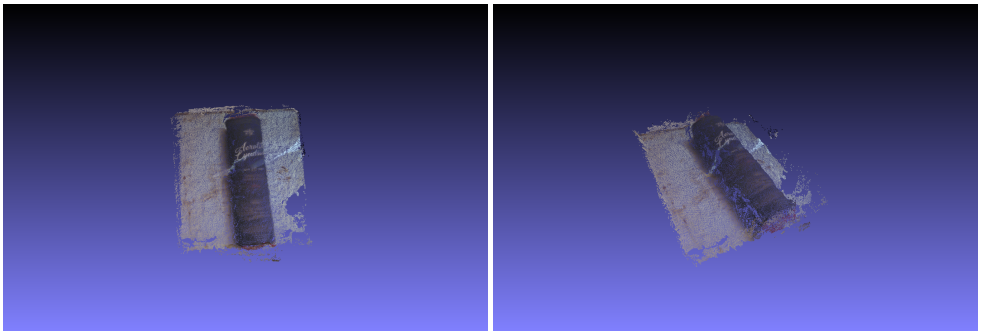

Figure 13. Representative side-view images of the real whisky bottle dataset.